HHS Public Access

Author manuscript

J Phys Chem Lett. Author manuscript; available in PMC 2017 August 30.

Published in final edited form as:

J Phys Chem Lett. 2017 June 01; 8(11): 2535–2540. doi:10.1021/acs.jpclett.7b01019.

Probing the Binding Modes of a Multidomain Protein to Lipid-based Nanoparticles by Relaxation-based NMR

Alberto Ceccon[†,§], **Vitali Tugarinov**[†,*,§], **Andrew J. Boughton**[‡], **David Fushman**[‡], and **G. Marius Clore**[†,*]

[†]Laboratory of Chemical Physics, National Institute of Diabetes and Digestive and Kidney Diseases, National Institutes of Health, Bethesda, Maryland 20892-0520, United States

[‡]Department of Chemistry and Biochemistry, Center for Biomolecular Structure and Organization, University of Maryland, College Park, Maryland 20742-4454, United States

Abstract

The interactions of two model multidomain proteins—covalently linked diubiquitins, Ub_2—with lipid-based nanoparticles have been quantitatively probed by the measurements of NMR lifetime line broadening, ΔR_2. By combined analysis of ΔR_2 profiles arising from interactions with liposomes of varying sizes, an approach recently developed for the characterization of interactions of monoubiquitin with liposomes, we determine how the parameters of exchange (liposome binding) and dynamics of each individual domain of Ub_2 on the surface of liposomes change when the domains are covalently attached to one another by a flexible linker. Two different covalent linkages were used: K63-linked and K48-linked Ub_2. The possibility of three distinct modes of binding of Ub_2 to liposomes requires the introduction of simple but important modifications to the strategy of analysis originally developed for monoubiquitin.

Graphical Abstract

[*]Corresponding Authors: G.M.C.: mariusc@mail.nih.gov., V.T.: vitali.tugarinov@nih.gov.
[§]Author Contributions
A.C. and V.T. contributed equally.
ORCID
David Fushman: 0000-0002-6634-8056
G. Marius Clore: 0000-0003-3809-1027

Notes

The authors declare no competing financial interest.

Supporting Information

The Supporting Information is available free of charge on the ACS Publications website at DOI: 10.1021/acs.jpclett.7b01019.
Details of sample preparation, NMR experiments, and fitting of the experimental data; Figures S1–S5. (PDF)

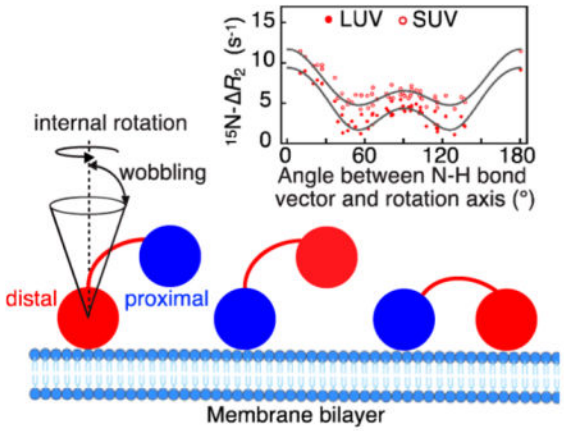

Reversible binding of peripheral membrane proteins to membrane surfaces is critical to many biological processes including signaling cascades, recognition, membrane trafficking, and anchoring.[1,2] Binding of these proteins is generally accomplished through lipid-interacting protein domains with or without penetration into the hydrophobic core of the membrane. While single-domain proteins or individual domains within multidomain proteins can adopt identical structures upon binding to cellular membranes, the characterization of the conformational states of multidomain proteins is more challenging as a description of the interplay between membrane-binding domains is required. Characterization of membrane binding and its influence on the dynamics of multidomain proteins therefore benefits from the application of atomic resolution techniques. With this in mind, we have undertaken a quantitative study of global dynamics and exchange kinetics of two multidomain model protein systems in the presence of lipid-based nanoparticles (liposomes).

Recently, we characterized the interaction of a model protein, ubiquitin, with the surface of negatively charged liposomes using relaxation-based NMR.[3] Because the relative contributions of lifetime and rotational tumbling to the total effective correlation time of the bound protein are modulated by nanoparticle size, parameters describing both exchange and dynamics can be determined simultaneously by quantitative analysis of lifetime line broadening (ΔR_2) profiles obtained with different sized nanoparticles. We showed that during the lifetime of the bound state (~20 μs) ubiquitin undergoes internal rotation on a time scale of ~2 μs about an axis approximately perpendicular to the lipid bilayer surface while simultaneously wobbling in a cone of semiangle 30–55° on a time scale <500 ns.[3]

Here we extend our previous work[3] to a more complex scenario in which the liposome-binding partner is a multidomain protein, as exemplified by covalently linked diubiquitin, Ub_2. Using ΔR_2 measurements, we explore how membrane binding and global dynamics of the individual domains on the surface of liposomes are impacted by two different, naturally occurring covalent linkages, Lys63- and Lys48-linked Ub_2. The rationale for our choice of linkages is based on their different conformational properties in solution: while K63-linked Ub_2 always adopts an extended conformation,[4,5] K48-linked Ub_2 has been shown to exist in both “closed” and “open” forms,[6–10] which interconvert on the tens of nanoseconds time

scale.[8,11] Because Ub_2 can potentially bind to liposomes in three distinct modes, simple but important modifications are required to the approach previously developed for monoubiquitin. Comparison of global parameters of exchange and dynamics obtained for the individual domains of K48- and K63-linked Ub_2 provides semiquantitative insights into the character of these binding modes and the interplay between the domains of Ub_2.

Covalently linked diubiquitin (Ub_2) is enzymatically generated through the formation of an isopeptide linkage between the ε-amine of an endogenous lysine side chain from one ubiquitin molecule (Ub_1), denoted as “proximal”, and the C-terminal carboxyl group of a second ubiquitin molecule, denoted as “distal”.[5,7] Because the $^{1}H_N/^{15}N$ chemical shifts of the proximal and distal domains are very similar, only a single domain of the K63- and K48-linked Ub_2 constructs was U- [$^{15}N/^{2}H$]-labeled at a time; the other remained at natural isotopic abundance (^{14}N), thereby ensuring that only a single domain at a time is observed in $^{1}H–^{15}N$ NMR correlation experiments. The details of Ub_2 ligation and isotope labeling are described in the Supporting Information (SI). Negatively charged large (LUV) and small (SUV) unilamellar vesicles (see the SI) had mean diameters of 112 and 28 nm, respectively, as measured by dynamic light scattering. The rotational correlation time (τ_R) for molecular reorientation of LUV and SUV liposomes, estimated from their hydrodynamic radii using the Stokes–Einstein equation, was 128.5 and 2.0 μs, respectively.

The experimental approach employed involves the measurement of lifetime line broadening (ΔR_2), given by the difference in transverse relaxation rates (R_2) of the protein measured in the presence and absence of nanoparticles. Lifetime line broadening arises from rapid decay of magnetization during the lifetime of the bound state that is transferred by exchange to the observable free state.[12,13] The ^{15}N-ΔR_2 profiles as a function of residue for the different Ub_2 constructs shown in Figure S1 reveal large variations in values ranging from a factor of ~3 for SUVs and ~10 for LUVs, similar to those observed for Ub_1 (Figure S2A). If Ub_1 and Ub_2 were immobilized on the lipid surface during their bound lifetime, then the measured ΔR_2 values would be uniform. The ^{15}N-ΔR_2 values are dependent both on nanoparticle size (Figure S3A) and magnetic field strength (Figure S3B). The average ratio of ^{15}N-ΔR_2 at 700 and 500 MHz is 1.19 (Figure S3B), in good agreement with the expected ratio of 1.20 for a relaxation mechanism based on a −170 ppm ^{15}N chemical shift anisotropy (CSA), allowing one to conclude that the field dependence of ΔR_2 does not arise from chemical exchange (which scales with the square of magnetic field) and that the exchange rate (k_{ex}) is fast on the transverse relaxation time scale (i.e., $k_{ex} > R_2^B$, where R_2^B is the ^{15}N transverse relaxation rate in the bound state).

In the absence of chemical shift differences between the free and bound states of the protein (none were observed in this work), the association of Ub_2 domains with liposomes is quantitatively described by a set of simplified Bloch–McConnell differential equations (SI eq S1). It is straightforward to show (see the SI for details) that, to a good approximation, for the interactions considered here, ΔR_2 can be represented by

$$\Delta R_2 \approx k_{\mathrm{on}}^{\mathrm{app}} \frac{R_2^{\mathrm{B}}}{k_{\mathrm{off}} + R_2^{\mathrm{B}}} \quad (1)$$

where k_{off} and $k_{\mathrm{on}}^{\mathrm{app}}$ are the dissociation and pseudo-first-order apparent association rate constants, respectively. The relaxation rates R_2^{B} are related to molecular motions of Ub_2 on the surface of liposomes through their dependence on linear combinations of the spectral density function $J(\omega)$ evaluated at a finite number of frequencies ω[14] (see SI eq S3 for the full expression for ^{15}N-R_2). All information about molecular dynamics is contained in the form and parameters of $J(\omega)$. As described in our previous work,[3] the variability in ^{15}N-ΔR_2 values of Ub_2 in the presence of liposomes can be explained by two concurrent motions of each domain on the surface of liposome particles: (1) internal rotation of a domain around an axis fixed in a molecular frame of reference and (2) the reorientation (wobbling) of the axis itself occurring on a time scale faster than internal rotation. The global motions of the protein on the nanoparticle surface can therefore be described by a form of the spectral density function that represents a variation of the extended model-free formalism[15] and is given by

$$J(\omega) = S_{\mathrm{w}}^2 [P_2(\cos\alpha)]^2 \frac{\tau_C}{1+(\omega\tau_{\mathrm{C}})^2} + S_{\mathrm{w}}^2 (1-[P_2(\cos\alpha)]^2) \frac{\tau_{\mathrm{r}}'}{1+(\omega\tau_{\mathrm{r}}')^2} + (1-S_{\mathrm{w}}^2) \frac{\tau_{\mathrm{w}}'}{1+(\omega\tau_{\mathrm{w}}')^2} \quad (2)$$

where $\tau_{\mathrm{C}} = (1/\tau_{\mathrm{R}} + 1/\tau_{\mathrm{ex}})^{-1}$ is the total effective correlation time; τ_{R} is the rotational correlation time of molecular reorientation of the complex; $\tau_{\mathrm{ex}} = (k_{\mathrm{on}}^{\mathrm{app}} + k_{\mathrm{off}})^{-1}$ is the lifetime of the bound state; $\tau_{\mathrm{r}}' = (1/\tau_{\mathrm{C}} + 1/\tau_{\mathrm{r}})^{-1}$ and $\tau_{\mathrm{w}}' = (1/\tau_{\mathrm{C}} + 1/\tau_{\mathrm{w}})^{-1}$ are the effective correlation times for internal rotation and wobbling on the nanoparticle surface, respectively, and τ_{r} and τ_{w} are the corresponding correlation times; S_{w} is the order parameter for wobbling within a cone centered about the internal rotation axis; and $P_2(\cos\alpha) = (3\cos^2\alpha - 1)/2$ is the second-order Legendre polynomial that represents the order parameter S_{r} for axially symmetric internal rotation around an axis forming an angle α with the direction of an N–H bond vector.

Internal rotation of ubiquitin about an axis fixed in the molecular frame results in a characteristic $S_{\mathrm{r}}^2 = [P_2(\cos\alpha)]^2$ dependence of R_2^{B} (and, consequently, ΔR_2) with two minima: at the magic angle, 54.7° (α = 54.7°) and 180° – 54.7° (α = 125.3°). The “double-dip” profiles of ^{15}N-ΔR_2 for Ub_1 in the presence of LUV and SUV liposomes at the same protein concentration and protein/lipid ratios as used here for the study of the Ub_2 domains are shown in Figure 1A and serve as a template for the analysis of similar dependencies observed for K63- and K48-linked diubiquitins (Figure 1B,C).

There are potentially three distinct binding modes of Ub_2 to the surface of liposomes (Figure 1D): (1) the U-[^{15}N/^{2}H]-labeled (“NMR-active”) domain is directly bound to the lipid bilayer; (2) the unlabeled (“NMR-silent”) Ub_2 domain binds, while the domain detected in

the NMR experiments is tethered; and (3) both "NMR-active" and "NMR-silent" domains bind simultaneously to the liposome surface. In the most general case, the overall experimentally measured lifetime line broadening, $\Delta R_2^{\mathrm{overall}}$, is therefore composed of a super-position of all of the possible binding modes and can be represented by

$$\Delta R_2^{\mathrm{overall}} = \Delta R_2 + F^{\mathrm{iso}} \quad (3)$$

where ΔR_2 is calculated using eq 1 (see also SI, eqs S1 and S2), the relaxation rates R_2^{B} are calculated using standard expressions (SI, eq S3) and the form of spectral density in eq 2, and F^{iso} is a uniform contribution to $^{15}\mathrm{N}-\Delta R_2^{\mathrm{overall}}$ that accounts for binding modes 2 and 3 (Figure 1D). One can assume that the tethered "NMR-observable" domain of Ub_2 (binding mode 2) behaves as an isotropic body and reorients fast relative to the bound domain on account of the relatively long and flexible linker connecting the two units of Ub_2, thus contributing a uniform, angle-independent value to ΔR_2. Furthermore, if binding mode 3 (both domains directly bound simultaneously) occurs in practice, then the rotation of each individual domain would be severely hindered by the covalent linkage between the two domains, also resulting in a uniform contribution to ΔR_2 because, in the absence of internal rotation, the large angular dependence of ΔR_2 would be eliminated. Indeed, even a cursory visual comparison of the "double-dip" ΔR_2 profiles for Ub_2 (Figure 1B,C) and Ub_1 (Figure 1A) shows that at least for some of the Ub_2 domains the profiles are simply "offset" by a positive uniform factor relative to those of Ub_1. In principle, there is no reason to assume that the value of F^{iso} should be the same for interactions of Ub_2 with LUV ($F_{\mathrm{LUV}}^{\mathrm{iso}}$) and SUV ($F_{\mathrm{SUV}}^{\mathrm{iso}}$) particles. Likewise, $F_{\mathrm{LUV}}^{\mathrm{iso}}$ and $F_{\mathrm{SUV}}^{\mathrm{iso}}$ can be different for distal and proximal domains of Ub_2 as well as for different types of linkages and should therefore be optimized separately for each Ub_2 domain (see below and the SI for details).

The key to interpretation of ^{15}N-ΔR_2 values for Ub_2 in terms of exchange ($k_{\mathrm{on}}^{\mathrm{app}}$ and k_{off} in eq 1) and microdynamic parameters (S_{r}^2, S_{w}^2, and corresponding correlation times in eq 2) lies in the *combined* use of the ^{15}N-ΔR_2 data obtained in the presence of vesicles of varying sizes (LUVs and SUVs). The working assumption employed here is that the global motional parameters and the dissociation rate constant are independent of particle size. Specifically, we require that the time scale of internal rotation τ_{r}, the polar angles (θ and φ) that describe the orientation of the internal rotation axis in a molecular frame of reference, the parameters of the wobbling motion (S_{w}^2 and τ_{w}), and the dissociation rate constant k_{off} are the same for binding to LUV and SUV particles. This approach allows one to quantitatively describe fast binding to liposomes while simultaneously establishing the parameters of global dynamics of the protein on the liposome surface. However, even combined analysis of LUV and SUV ΔR_2 data precludes the determination of the wobbling parameters, S_{w}^2 and τ_{w}, as the product of the order parameters for internal rotation and wobbling enter into the first and second terms of the spectral density function in eq 2. Therefore, all exchange and dynamics parameters reported here were obtained with S_{w}^2 and τ_{w} set to values of 0.5 and 300 ns,

respectively. We note that these parameters are quite insensitive to the exact values of S_w^2 and τ_w, whose lower and upper bounds were established previously for Ub_1–liposome complexes via extensive grid-searches in the parameter space covered by interactions with LUV and SUV liposomes separately.[3]

The variability of ΔR_2 experimental values for each domain of Ub_2 (see Figure S1, which shows the ΔR_2 profiles versus residue number) can be defined by the ratio R

$$R=(\Delta R_2^{\max}-F^{\mathrm{iso}})/(\Delta R_2^{\min}-F^{\mathrm{iso}}) \quad (4)$$

For the same wobbling motion parameters (S_w^2 and τ_w) R is predicated upon the degree of separation between the time scale of internal rotation (τ_r) and the total effective correlation times for LUV (τ_C^{LUV}) and SUV (τ_C^{SUV}) particles. The larger the separation between τ_C and τ_r, the larger the variability in the ratio R. In contrast to Ub_1, where F^{iso} = 0, the calculated value of R in the case of Ub_2 depends on the value of F^{iso} and therefore provides a good measure of the separation between the τ_C and τ_r time scales (see below).

Not all fitted parameters are well-defined from combined analysis of the SUV and LUV ΔR_2 data for the Ub_2 domains owing to (a) the reduced variability of ΔR_2 values (i.e., $\Delta R_2^{\max}/\Delta R_2^{\min}$ before the "isotropic" contributions F^{iso} are taken into account) for at least some of the Ub_2 domains and (b) the interdependence of various variable parameters (see below). Therefore, to preserve the robustness of analysis for all domains and linkage types of Ub_2 and to enable direct comparison of the dynamics parameters obtained for different Ub_2 domains, we chose to determine the values of $k_{on}^{\mathrm{app,LUV}}$ for the different Ub_2–LUV interactions independently from paramagnetic relaxation enhancement (PRE) experiments (Figure 2).[16] Outside the fast exchange regime ($k_{ex} < \Gamma_2$, where Γ_2 is the PRE rate in the bound species), the maximal observed PRE, $^1\mathrm{H_N}-\Gamma_{2,\max}^{\mathrm{app}}$, after background subtraction,[3] approaches a limiting value that is a factor of ~1.3 lower than $k_{on}^{\mathrm{app,LUV}}$ for the exchange parameters previously established for Ub_1.[16] The values of $k_{on}^{\mathrm{app,LUV}}$ thus estimated from $^1\mathrm{H_N}-\Gamma_{2,\max}^{\mathrm{app}}$ for each Ub_2 domain are reported in the first row of Table 1, which summarizes the parameters of exchange and dynamics obtained by combined analysis of LUV and SUV ΔR_2 data for the distal/proximal domains of K63- and K48-linked Ub_2.

The intermolecular amide proton PRE ($^1\mathrm{H_N}-\Gamma_2^{\mathrm{app}}$) profiles shown in Figure 2 for the distal and proximal domains of K63- and K48-linked Ub_2 in the presence of Gd^{3+}-tagged LUVs indicate that the regions with the most significant PREs largely coincide with those measured for Ub_1–LUV complexes (Figure S2B). Thus the location of the binding surface remains largely unchanged in individual domains of Ub_2 relative to Ub_1.

The details of the construction of the target error function and its minimization are described in the SI. In brief, because per eqs 1 and 3 $F_{\mathrm{LUV}}^{\mathrm{iso}}$ and $F_{\mathrm{SUV}}^{\mathrm{iso}}$ are linearly correlated with the

corresponding association rate constants for LUV and SUV particles, $k_{on}^{app,LUV}$ and $k_{on}^{app,SUV}$ (see the SI for full expressions), it is not possible to determine k_{on}^{app} and F^{iso} simultaneously. Therefore, we first performed the analysis with $k_{on}^{app,LUV}$ fixed to the values determined as described above and assumed that $F_{LUV}^{iso}=F_{SUV}^{iso}$. This allowed us to obtain optimal estimates for $k_{on}^{app,SUV}$ for each of the Ub_2 domains (listed as upper bounds in Table 1). Subsequently, the values of $k_{on}^{app,SUV}$ obtained in this manner were reduced by four times the uncertainty in the fit (listed as lower bounds in Table 1), and F_{SUV}^{iso} was used as an optimized parameter in the fit, providing the upper bounds for F_{SUV}^{iso} listed in Table 1. Note that the upper bounds determined for F_{SUV}^{iso} thus correspond to the lower bounds for $k_{on}^{app,LUV}$ and τ_r values, whereas the lower bounds for F_{SUV}^{iso} are equal to F_{LUV}^{iso} (Table 1).

Figure 3 compares the orientations of Ub_1 and the domains of Ub_2 on the surface of liposomes, with the axes of internal rotation aligned in the direction perpendicular to the lipid bilayer. The positions of the internal rotation axes of Ub_1 and the distal and proximal domains of the K48-linked Ub_2 in the coordinate system of the inertia tensor of ubiquitin are illustrated in Figure 3C. The orientations of the Ub_2 domains on the lipid bilayer surface are very similar to that of Ub_1 (Figure 3A,B; Table 1), with the angles ω' and ω'' formed between the internal rotation axes of Ub_1 and the distal and proximal domains of Ub_2 (Figure 3C) calculated to be 6.1 and 14.5°, respectively, for K63-linked Ub_2 and 4.9 and 18.2° for K48-linked Ub_2. Some differences, however, in the binding affinities and the parameters of dynamics on the surface of liposomes are noteworthy. First, the positions of the axes of internal rotation (defined by the pair of polar angles θ and ϕ) of the distal domains are closer to Ub_1 than those of the proximal domains. Second, the affinity of the distal domains for liposomes is very similar to that of Ub_1 and larger than for their proximal counterparts, as evidenced by their higher bound occupancies (cf. populations of the bound states, p_B, for LUVs and SUVs in Table 1). These two observations imply that perturbations of the liposome-binding surface arising from the linkages in Ub_2 are more pronounced for the proximal than distal domains. This is a direct consequence of the fact that the distal domains are connected to the proximal ones through a flexible and unstructured C-terminus. As a result, the binding interface on the distal domains remains almost intact in the presence of the isopeptide linkage; the latter, however, can lead to a partial occlusion of the binding interface in the case of proximal domains.

A comparison of the binding and kinetic parameters for the K63- and K48-linked Ub_2 is equally instructive, as the former exists exclusively in an extended conformation in solution,[4,5] whereas the latter is a mixture of rapidly interconverting open and closed states.[6–11,17] Mapping of the amide proton intermolecular PREs on the surface of K48- and K63-linked Ub_2 shows that the lipid binding surface on both domains is fully accessible in the open state but completely occluded in the closed one (Figure S4). The ability of the K48-linked Ub_2 to adopt, for at least a small fraction of the time, a liposome-binding incompetent (closed) state may be reflected in slightly larger values of F^{iso} for the K48- versus K63-linked Ub_2 (Table 1), indicating that binding modes (2) and (3) (cf. Figure 1D) play a slightly more important role when Ub_2 is capable of transiently adopting a closed

conformation. The degree of association between the Ub_2 domains may also be related to the observation of somewhat lower values of the internal rotational time scale (τ_r) for K63-linked Ub_2 compared with those of K48-linked Ub_2 (Table 1). Note that lower values of τ_r correspond to higher values of the ratio R (eq 4), as the latter depend on the separation between τ_r and the effective correlation times of LUV and SUV particles (Figure S5).

In conclusion, we have provided a theoretical framework for the quantitative description of the dynamics of two (K48- and K63-linked) diubiquitins on the surface of liposome nanoparticles. The formalism extends our previous work on monoubiquitin[3] involving various modes of binding including direct contact and tethered binding of a single domain and simultaneous binding of both domains. It has not escaped out attention that more rigorous (i.e., non-model-free) formulations of the spectral density function (eq 2) are possible if the nature of the motion of the protein on the liposome surface is specified. Indeed, much earlier, Brainard and Szabo[18] derived an expression for a correlation function describing rotation of a bond vector around a symmetry axis defined in the molecular frame with the axis undergoing diffusive motions (i.e., wobbling) about its equilibrium position (see the SI). The use of the corresponding spectral density function (eq S9, SI) yields parameters of exchange and dynamics that are very similar to those reported in Table 1 (using eq 2) and does not affect any of the conclusions of the present work.

Supplementary Material

Refer to Web version on PubMed Central for supplementary material.

Acknowledgments

We thank James Baber, Dan Garrett, and Jinfa Ying for technical support. This work was supported by the Intramural Program of NIDDK, NIH and by the AIDS Targeted Antiviral program of the Office of the Director of the NIH (to G.M.C.).

References

1. Cho W, Stahelin RV. Membrane-Protein Interactions in Cell Signaling and Membrane Trafficking. Annu Rev Biophys Biomol Struct. 2005; 34:119–151. [PubMed: 15869386]
2. Di Paolo G, De Camilli P. Phosphoinositides in Cell Regulation and Membrane Dynamics. Nature. 2006; 443:651–657. [PubMed: 17035995]
3. Ceccon A, Tugarinov V, Bax A, Clore GM. Global Dynamics and Exchange Kinetics of a Protein on the Surface of Nanoparticles Revealed by Relaxation-Based Solution NMR Spectroscopy. J Am Chem Soc. 2016; 138:5789–5792. [PubMed: 27111298]
4. Tenno T, Fujiwara K, Tochio H, Iwai K, Morita EH, Hayashi H, Murata S, Hiroaki H, Sato M, Tanaka K, Shirakawa M. Structural Basis for Distinct Roles of Lys63- and Lys48-Linked Polyubiquitin Chains. Genes Cells. 2004; 9:865–875. [PubMed: 15461659]
5. Varadan R, Assfalg M, Haririnia A, Raasi S, Pickart C, Fushman D. Solution Conformation of Lys63-Linked Diubiquitin Chain Provides Clues to Functional Diversity of Polyubiquitin Signaling. J Biol Chem. 2003; 279:7055–7063. [PubMed: 14645257]
6. Cook WJ, Jeffrey LC, Carson M, Chen Z, Pickart CM. Structure of a Di-Ubiquitin Conjugate and a Model for Interaction with Ubiquitin Conjugating Enzyme (E2). J Biol Chem. 1992; 267:16467–16471. [PubMed: 1322903]
7. Varadan R, Walker O, Pickart C, Fushman D. Structural Properties of Polyubiquitin Chains in Solution. J Mol Biol. 2002; 324:637–647. [PubMed: 12460567]

8. Ryabov Y, Fushman D. Structural Assembly of Multidomain Proteins and Protein Complexes Guided by the Overall Rotational Diffusion Tensor. J Am Chem Soc. 2007; 129:7894–7902. [PubMed: 17550252]
9. Hirano T, Serve O, Yagi-Utsumi M, Takemoto E, Hiromoto T, Satoh T, Mizushima T, Kato K. Conformational Dynamics of Wild-Type Lys-48-Linked Diubiquitin in Solution. J Biol Chem. 2011; 286:37496–37502. [PubMed: 21900242]
10. Berlin K, Castaneda CA, Schneidman-Duhovny D, Sali A, Nava-Tudela A, Fushman D. Recovering a Representative Conformational Ensemble from Underdetermined Macromolecular Structural Data. J Am Chem Soc. 2013; 135:16595–16609. [PubMed: 24093873]
11. Ryabov YE, Fushman D. A Model of Interdomain Mobility in a Multidomain Protein. J Am Chem Soc. 2007; 129:3315–3327. [PubMed: 17319663]
12. Fawzi NL, Ying J, Torchia DA, Clore GM. Kinetics of Amyloid β Monomer-to-Oligomer Exchange by NMR Relaxation. J Am Chem Soc. 2010; 132:9948–9951. [PubMed: 20604554]
13. Fawzi NL, Ying J, Ghirlando R, Torchia DA, Clore GM. Atomic-Resolution Dynamics on the Surface of Amyloid-β Protofibrils Probed by Solution NMR. Nature. 2011; 480:268–272. [PubMed: 22037310]
14. Abragam, A. Principles of Nuclear Magnetic Resonance. Clarendon Press; Oxford, England: 1961.
15. Clore GM, Szabo A, Bax A, Kay LE, Driscoll PC, Gronenborn AM. Deviations from the Simple Two-Parameter Model-Free Approach to the Interpretation of ^{15}N Nuclear Magnetic Relaxation of Proteins. J Am Chem Soc. 1990; 112:4989–4991.
16. Ceccon A, Clore GM, Tugarinov V. Towards Interpretation of Intermolecular Paramagnetic Relaxation Enhancement Outside the Fast Exchange Limit. J Biomol NMR. 2016; 66:1–7. [PubMed: 27558624]
17. Lai MY, Zhang D, Laronde-Leblanc N, Fushman D. Structural and Biochemical Studies of the Open State of Lys48-Linked Diubiquitin. Biochim Biophys Acta –Mol Cell Res. 2012; 1823:2046–2056.
18. Brainard JR, Szabo A. Theory for Nuclear Magnetic Relaxation of Probes in Anisotropic Systems: Application of Cholesterol in Phospholipid Vesicles. Biochemistry. 1981; 20:4618–4628. [PubMed: 7197547]

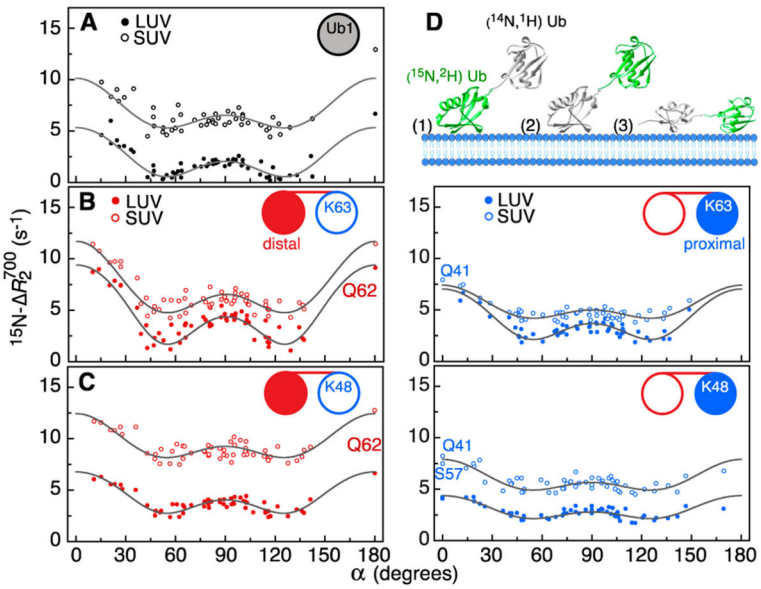

Figure 1.

^{15}N-ΔR_2 values plotted versus the angles α formed between the H–N bond vectors and the axis of internal rotation for (A) monoubiquitin (Ub_1) and the distal and proximal domains of (B) K63- and (C) K48-linked diubiquitin (Ub_2). Experimental data points are shown as solid and open circles for negatively charged LUVs and SUVs, respectively. The best-fit curves from the combined analysis of the LUV and SUV data (with S_w^2 and τ_w set to 0.5 and 300 ns, respectively) are shown with black lines. The [^{15}N/^{2}H]-labeled domains of Ub_2 are shown as filled-in circles with the distal and proximal domains of Ub_2 in red and blue, respectively, in the cartoons within each panel. (D) Schematic representation of the three potential binding modes of Ub_2 to lipid-based nanoparticles with the [^{15}N/^{2}H]-labeled ("NMR-active") domain shown in green. All experimental data were collected at 700 MHz on samples containing 0.22 mM protein and a 1:2 protein/lipid molar ratio at pH 6.8 and 25 °C.

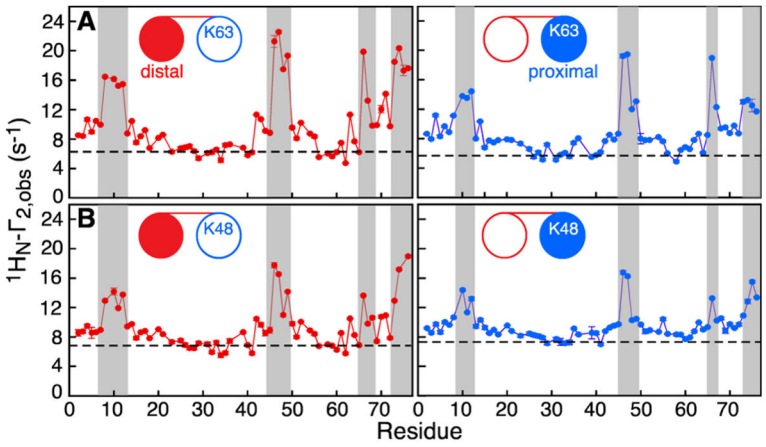

Figure 2.

Amide proton intermolecular PRE profiles obtained at 700 MHz. (A) K63- and (B) K48-linked Ub_2 in the presence of negatively charged Gd^{3+}-tagged negatively charged LUVs. The [$^{15}N/^2H$]-labeled domains of Ub_2 are shown with filled-in circles in the cartoons, and the distal and proximal domains are depicted in red and blue, respectively. The PRE background, due to diffusion of Ub_2 in the magnetic field generated by Gd^{3+}-tagged LUVs,[3] is shown as a dashed line. The most significant PREs above background are shaded in gray. Sample conditions are as in Figure 1.

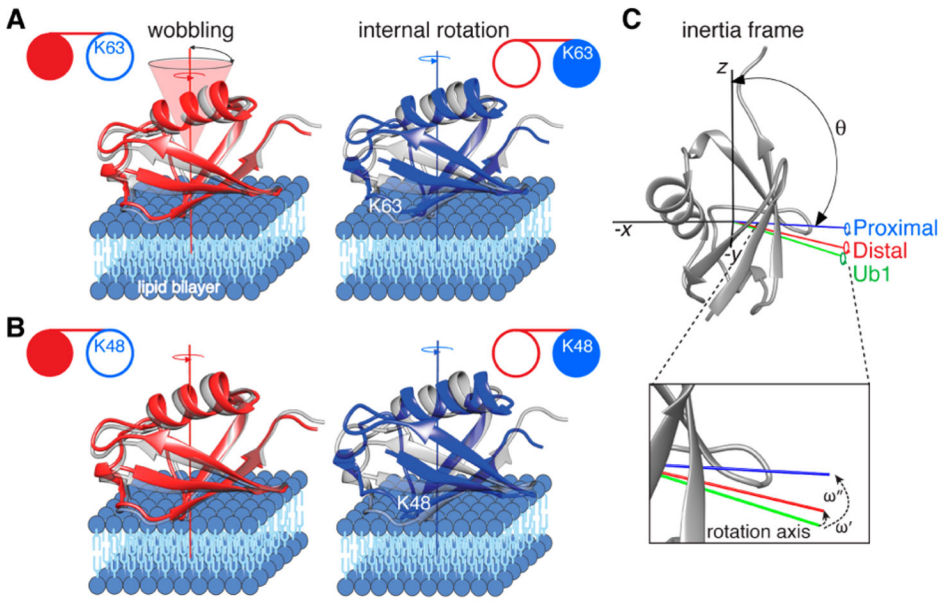

Figure 3.

Internal rotation and wobbling of the proximal and distal domains of Ub_2 on the surface of lipid-based nanoparticles. (A) K63- and (B) K48-linked Ub_2. The distal and proximal domains of Ub_2 are shown as red and blue ribbons, respectively, with Ub_1 in gray for comparison. Each domain rotates about an internal axis of rotation, approximately perpendicular to the lipid bilayer, and simultaneously wobbles in a cone centered around this axis. (C) Relationship between the axes ($-x$, $-y$, and z) of the inertia tensor (black) in the molecular frame with the internal rotation axes of Ub_1 (green) and the distal (red) and proximal (blue) domains of K48-linked Ub_2. θ is the angle subtended by each internal rotation axis and the z axis of the intertia tensor; φ (not shown) is the angle subtended by the x axis of the inertia tensor and the projection of the internal rotation axis on the x–y plane. The angle formed between the internal rotation axis of Ub_1 (green) and those of the distal (red) and proximal (blue) domains of Ub_2 are denoted by ω' and ω'', respectively. These angles are calculated from the polar angles (θ_i, φ_i) defining the position of axis i (i = 1,2) in the inertia frame using the relationship $\cos(\omega) = \cos(\theta_1)\cos(\theta_2) + \sin(\theta_1)\sin(\theta_2)\cos(\varphi_1 - \varphi_2)$. The U-[^{15}N/^{2}H]-labeled domains of Ub_2 are shown as filled-in circles in the cartoons in panels A and B.

Table 1

Parameters of Exchange and Dynamics Describing the Interactions of K63- and K48-Linked Ub_2 with LUV and SUV Liposomes at pH 6.8, 25°C and 1:2 Ubiquitin/Lipid Molar Ratio[a,b]

	K63-linked Ub_2		K48-linked Ub_2	
parameters	**distal**	**proximal**	**distal**	**proximal**
$k_{on}^{app,LUV}\ (s^{-1})$	21	18	14	13
$k_{on}^{app,SUV}\ (s^{-1})$	197–211	116–144	195–239	162–210
$k_{off} \times 10^3\ (s^{-1})$	32 ±1	40 ±1	36 ±1	55 ± 3
$p_B^{LUV}\ (\%)_c$	0.07	0.04	0.04	0.02
$p_B^{SUV}\ (\%)_c$	0.65 ± 0.03	0.32 ± 0.04	0.58 ± 0.07	0.35 ± 0.05
$\tau_C^{LUV}\ (\mu s)_c$	25.2 ± 0.8	21.0 ± 0.4	22.5 ± 0.9	16.0 ± 0.8
$\tau_C^{SUV}\ (\mu s)_c$	1.9 ± 0.2	1.9 ± 0.2	1.9 ± 0.2	1.8 ± 0.2
$\tau_r\ (\mu s)$	0.4–0.6	0.4–1.0	1.2–2.0	0.6–1.4
θ (deg)[d]	102.7 ± 0.7	98.4 ± 0.9	103.9 ± 0.8	93.5 ± 1.2
φ (deg)[d]	−5.3 ± 0.7	−13.7 ± 0.7	−5.1 ± 0.9	−13.7 ± 1.0
$F_{LUV}^{iso}\ (s^{-1})$	1.3 ± 0.1	1.7 ± 0.1	2.1 ± 0.1	1.9 ± 0.1
$F_{SUV}^{iso}\ (s^{-1})$	1.3–2.0	1.7–3.0	2.1–4.3	1.9–3.4
R_{SUV}[e]	4.2	4.1	2.6	3.7

[a] All reported the values are obtained with S_w^2 and τ_w fixed at 0.5 and 300 ns, respectively; throughout, the upper bounds reported for F_{SUV}^{iso} correspond to the lower bounds for $k_{on}^{app,SUV}$ and τ_r values in Ub_2 domains (see the text for details).

[b] For comparison, the values of $k_{on}^{app,LUV}$, $k_{on}^{app,SUV}$, k_{off}, τ_r, θ, and φ for Ub_1 are 27 s^{-1}, 347 ± 14 s^{-1}, 52(±1.9) × 10^3 s^{-1}, 1.5 ± 0.2 μs, 108.4 ± 1.1°, and −2.5 ± 1.1°, respectively.

[c] Uncertainties in these parameter values are propagated considering only the uncertainties in k_{off}. Uncertainties in the values of p_B^{LUV} are equal to ~0.002.

[d] Polar angles θ and φ are specified in the coordinate system of the inertia tensor of ubiquitin (PDB accession code 1ubq).

[e] Calculated for Ub_2–SUV complexes using the experimental values of $\Delta R_{2,SUV}$ and the upper bounds of the fitted F_{SUV}^{iso} values.